https://doi.org/10.1016/j.ijrmhm.2015.12.002

This is the Pre-Published Version.

Surface Generation Mechanism of WC/Co and RB-SiC/Si Composites under High Spindle Speed Grinding (HSSG)

Quanli Zhang[a,b], Suet To[b*], Qingliang Zhao[a], Bing Guo[a]

[a] *Centre for Precision Engineering, School of Mechatronics Engineering, Harbin Institute of Technology, Harbin, 150001, China*

[b] *State Key Laboratory of Ultra-precision Machining Technology, The Hong Kong Polytechnic University, Hong Kong, China*

Correspondent author: Suet To

Corresponding address: *State Key Laboratory of Ultra-precision Machining Technology, The Hong Kong Polytechnic University, Hong Kong, China*

Tel: +852-2766 6587; Fax: +852-2764 7657

E-mail: *sandy.to@inet.polyu.edu.hk*

Abstract

The surface generation mechanisms of WC/Co and Reaction-bonded SiC/Si (RB-SiC/Si) composites under high spindle speed grinding (HSSG) were investigated in the present work, compared with quasi-static indentation test. The results showed that surface generation mechanism for WC/Co and RB-SiC/Si varied under both quasi-static indentation and dynamic grinding. Only plastic deformation occurred for WC/Co indicating its higher toughness, while pop-out effect induced by phase transformation in RB-SiC/Si would prompt the chipping at phase boundaries under indentation. Under dynamic grinding, WC/Co underwent plastic deformation, grain dislodgement and WC particles crush, while ductile removal, phase boundaries crack (along the grinding direction) and chipping fracture occurred for RB-SiC/Si with the increase of cutting depth. It was found that the binder in the bulk WC/Co and RB-SiC/Si played a decisive role on the material removal mode, and the mechanics of grain dislodgement for WC/Co and RB-SiC/Si were analyzed based on a geometrical model. Besides, three types of grinding wheel wear appeared, including grit dislodgement, flattening and splintering, which bear an obvious influence on the surface generation.

Keywords: High spindle speed grinding; surface generation mechanism; composites; wheel wear

© 2016. This manuscript version is made available under the CC-BY-NC-ND 4.0 license http://creativecommons.org/licenses/by-nc-nd/4.0/

1. Introduction

Tungsten carbide (WC) and silicon carbide (SiC) are extensively used in optical mold and electronic industries for their excellent mechanical properties at high temperature, such as high stability, corrosion resistance, high strength and hardness [1-5]. Unfortunately, great challenge still exists in obtaining devices of high accuracy since the surface and subsurface damage could be easily induced during the machining process [6, 7], and there is great difficulty in machining them for their high hardness and brittleness by single point diamond turning (SPDT). Ultra-precision grinding is now considered as the most appropriate and best method to machining them [8], but a damage layer seems to be inevitable. A great number of studies have been focused on the grinding induced surface and subsurface damage caused by the interaction between the abrasive grit and workpiece materials, such as the surface fracture [9, 10], phase transformation [11, 12], residue stress [7, 13], subsurface cracks [13, 14] and edge chipping [2, 15]. These damage forms are all closely related to the material removal mechanism [16].

Brittle and ductile regime material removal during grinding were reported during machining of hard and brittle materials [17, 18]. Under ultra-precision grinding, WC is characterized by plastic deformation and scratching grooves, which is thought to be an indication of ductile material removal [9, 19-21], while the surface feature for SiC is mainly fracture and cracks [10, 14, 22-25], indicating the brittle material removal mode. Mechanical condition for brittle to ductile transition has been widely investigated by micro-indentation test and scratch. The critical load for ductile mode machining could be built by this quasi-non-destructive technique [26, 27], as well as the surface and subsurface damage induced during grinding [12, 28, 29]. Above all, the material microstructure

plays a critical role on its mechanical properties and machinability, then it is certain that the material removal and surface generation mechanism of WC and SiC should also have been changed accordingly after the addition of Co and Si, respectively [1, 30]. Unfortunately, few research has been conducted to investigate its influence on material removal mechanism under grinding directly, as well as the comparison of difference for WC/Co and RB-SiC/Si at each stage of grinding process.

In the present paper, indentation test was firstly performed to illustrate the quasi-static indentation induced damage, and then the material removal mechanism of WC/Co and RB-SiC/Si composites under high spindle speed grinding (HSSG) was investigated by a novel plunge grinding methodology, taking into account of the diamond grits wear. The mechanics of each material removal stage for WC/Co and RB-SiC/Si are then analyzed, and the difference is illustrated and explained based on a proposed geometric model.

2. Experimental procedures

2.1 Materials and machine

Table 1. Mechanical properties of workpiece materials

Workpiece	RB-SiC/Si	WC/Co
Elastic modulus E (GPa)	410	600
Vikers hardness H (kgf mm^{-2})	2500	1550
Fracture toughness K_{IC} (MPa m$^{1/2}$)	3.0 [14, 22]	8-11.0 [31]
Compressive strength (MPa)	2000	5500
Composition (wt.%)	Si~10.0	Co~6.0
Density ρ (g/cm^3)	3.1	14.95
Size of workpiece (mm)	16×16×5	12×12×5

Commercially available RB-SiC/Si and WC/Co composites (Goodfellow Cambridge Ltd., UK) were chosen as the workpiece materials. To manufacture RB-SiC/Si and WC/Co composites, silicon and cobalt is added into WC and SiC/C powder green body, respectively, which is then fired. The

resulting microstructure of both RB-SiC/Si and WC/Co has low porosity and fine grain, in which about 10.wt% and 6.wt% residue Si and Co worked as binders, respectively, and the SiC particle is about 10 μm and WC grain about 2 μm. As is shown in Fig. 1, WC/Co is composed of WC and Co phases, with only a small amount of CoO. While for RB-SiC/Si composite, five main phases exist in the bulk materials, including Si, 6H-SiC, 3C-SiC, 4H-SiC and SiO_2. The oxide might be produced during firing stage and remained in the surface of original bulk materials. Table 1 describes the mechanical properties of RB-SiC/Si and WC/Co composites. The workpiece materials were firstly polished with diamond paste of 1 μm diameter to remove the surface layer and reduce the impact of the original surface defects. The roughness of polished surface was about 5 nm and 10 nm for WC/Co and RB-SiC/Si composites, respectively. Ultra-precision plunge grinding was conducted on Moore Nanotech 450UPL, equipped with an on-machine measuring probe. Illustration of the grinding machine is shown in Fig. 2. The workpiece was fixed on a tilted-α fixture, with the workpiece and wheel rotating both counterclockwise. Resin-bonded wheel of 1500# grit size (Diagrind, Inc., USA) was chosen for creep-plunge grinding after appropriate truing and dressing. The detail machining parameters are listed in Table 2.

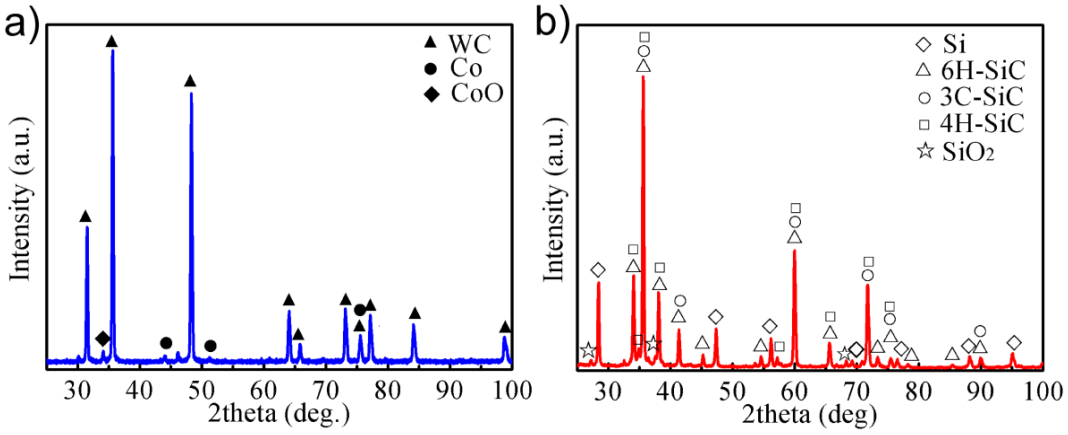

Fig. 1 X-ray diffraction pattern and phase composition of the original materials: (a) WC/Co, (b) RB-SiC/Si

Based on previous studies [32, 33], the force during micro-grinding with high spindle speed is in the level of 0.1 kgf, so the Vickers indentation under 0.1 kg is conducted to compare the indentation results with grinding experiments. Specifically, three times of indentation were conducted on the polished original materials surface by Vickers micro-hardness tester (MicroWiZhard), with the loading time of 5 s, holding time of 10 s and unloading time 5 s.

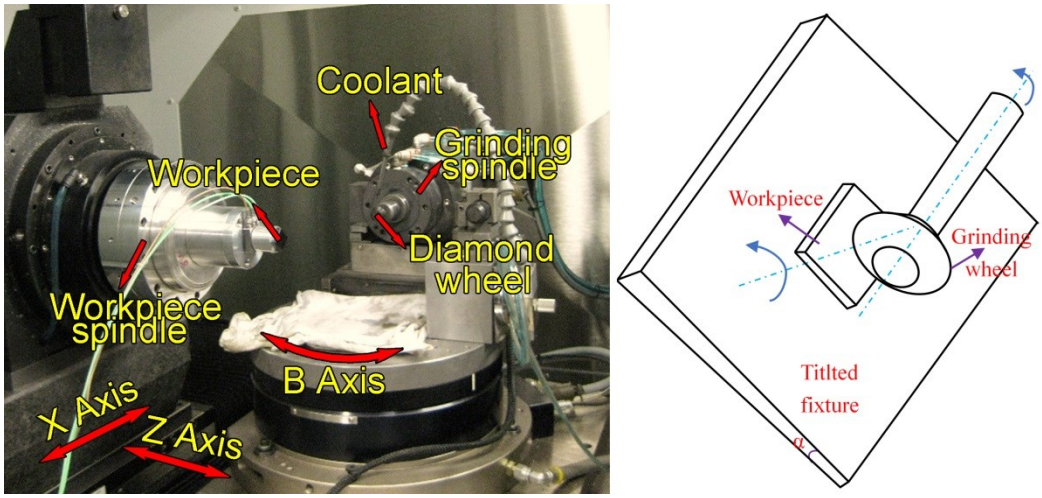

Fig. 2 Schematic of plunge grinding setup

Table 2. Plunge micro-grinding parameters

Wheel(20mm in diameter)	1500#G0787B195
Coolant	CLAIRSOL 350
Wheel *RPM* (rpm)	20,000
Workpiece *RPM* (rpm)	1

2.2 Characterization and measurement

The phase composition of original materials was analyzed by X-ray diffraction (XRD, Rigaku SmartLab) with CuKα radiation (45 kV, 200mA). The scanning angle of X-ray was chosen to be 25 to 100 deg. and the XRD spectrum was analyzed by Jade 6.5 software. The morphology of the indentation dimples, grinding surfaces and wheel surface after grinding were characterized by scanning electron microscope (SEM, Hitachi TM3000). Surface topography of each indentation

dimple was then measured by atomic force microscope (AFM, Park's XE-70). Nexview 3D profilers (ZygoLamda) was used to examine the typical 3D surface topography of 1500# diamond wheel after grinding, while the cross-sectional profile of the plunge grinding trace was analyzed by the white light interferometer (Wyko NT8000) with vertical scanning interferometry in a range of 154.5×115.9 μm.

3. Results

Before the grinding process being conducted, the wheel was first trued by a diamond nib on the workpiece spindle. As is shown in Fig. 3, the grinding wheel with 60° degree sharp edge could be obtained after truing and dressing process. The achieved sharp edge radius of grinding wheel was about 20 μm. Therefore, much less diamond grains would be involved in the cutting process which was helpful in analyzing and tracking the cutting trajectory of individual diamond grits.

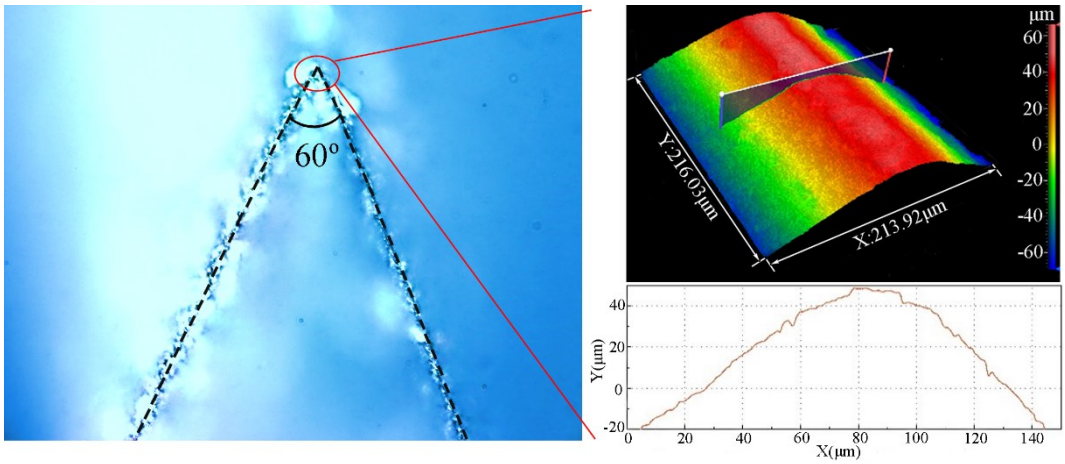

Fig. 3 Sharp edge of grinding wheel after truing by diamond nib

Fig. 4 shows the indentation profile on WC/Co and RB-SiC/Si. Regular deformed indentation dimples were produced on WC/Co and no apparent crack was generated. On the contrary, evident cracks occurred at each indentation position on RB-SiC/Si. Furthermore, the varied size of

impression was resulted from the varied hardness of SiC and Si. The topography of each indentation dimple was shown in Fig. 5. It could be easily found that the shape of three indentations left on WC/Co was uniform, and no obvious extrusion of workpiece material appeared at the pit edge. For RB-SiC/Si, the pop-out phenomenon occurred for each dimple. To be more specific, the swell and the accompanied lateral crack mainly appeared at the phase boundaries between SiC and Si.

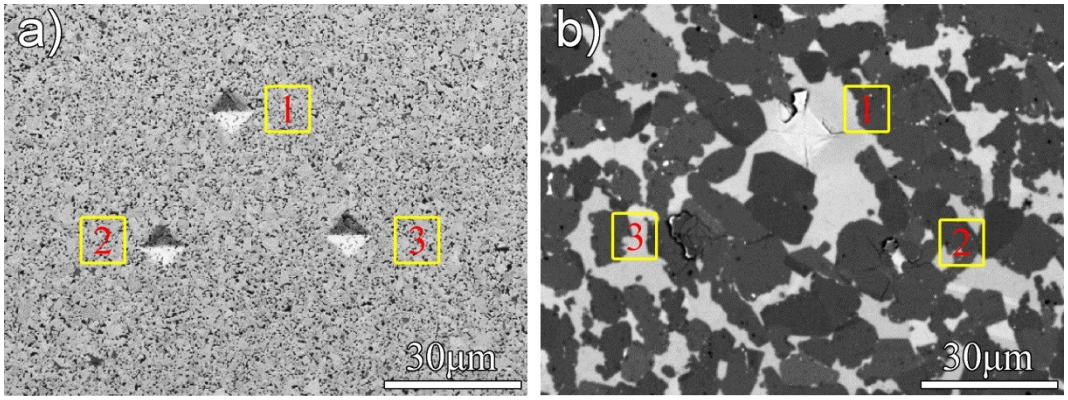

Fig. 4 Vickers-hardness indentation profile on WC/Co and RB-SiC/Si composites

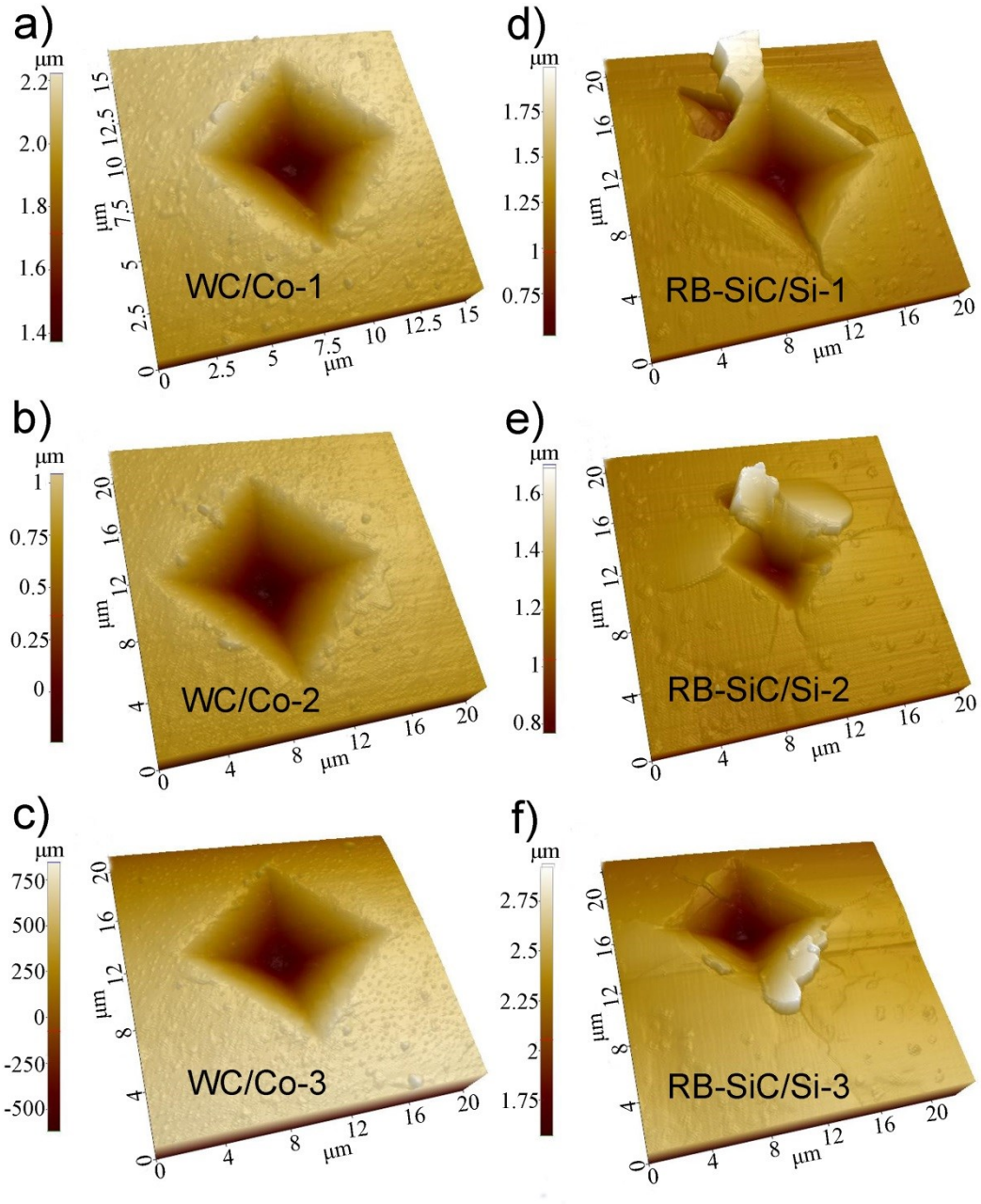

Fig. 5 Topography of the Vickers-hardness indentation profile: (a) WC/Co-1, (b) WC/Co-2, (c) WC/Co-3; (d) RB-SiC/Si-1, (e) RB-SiC/Si-2, (f) RB-SiC/Si-3

As is shown in Fig. 6, the machined surface of both WC/Co and RB-SiC/Si carbides were characterized with plastic scratching groove at the very beginning of the grinding process (indicated by the pink arrows). However, things differed with the increasing depth of cut. For WC/Co, WC particles were extruded to be denser under the impact pressure of diamond grits (indicated by yellow

ellipses), while the extruded Co binder between the neighboring hard phases was removed with less binder remained. Afterwards, some of the WC grains were crushed as the depth of cut for parts of grits involved in cutting became greater than the critical depth (indicated by red rectangles). For RB-SiC/Si, the ductile removal appeared on the surface of both SiC and Si phases at the beginning, but discontinuous micro-pits at the SiC and Si phase boundaries along the grinding direction were induced under the pressure of diamond grits. Worse, non-regular surface fragmentation occurred (indicated by yellow curves), and the surface quality was aggravated by the breaking and tearing of workpiece materials with the increasing cutting depth. Besides, although more diamond grits were involved in cutting the workpiece material with the increase of depth of cut, the material removal mode for a single grit differed from each other considering the surface profile of wheel and random protruding height of grits, which can be seen from Fig. 6.

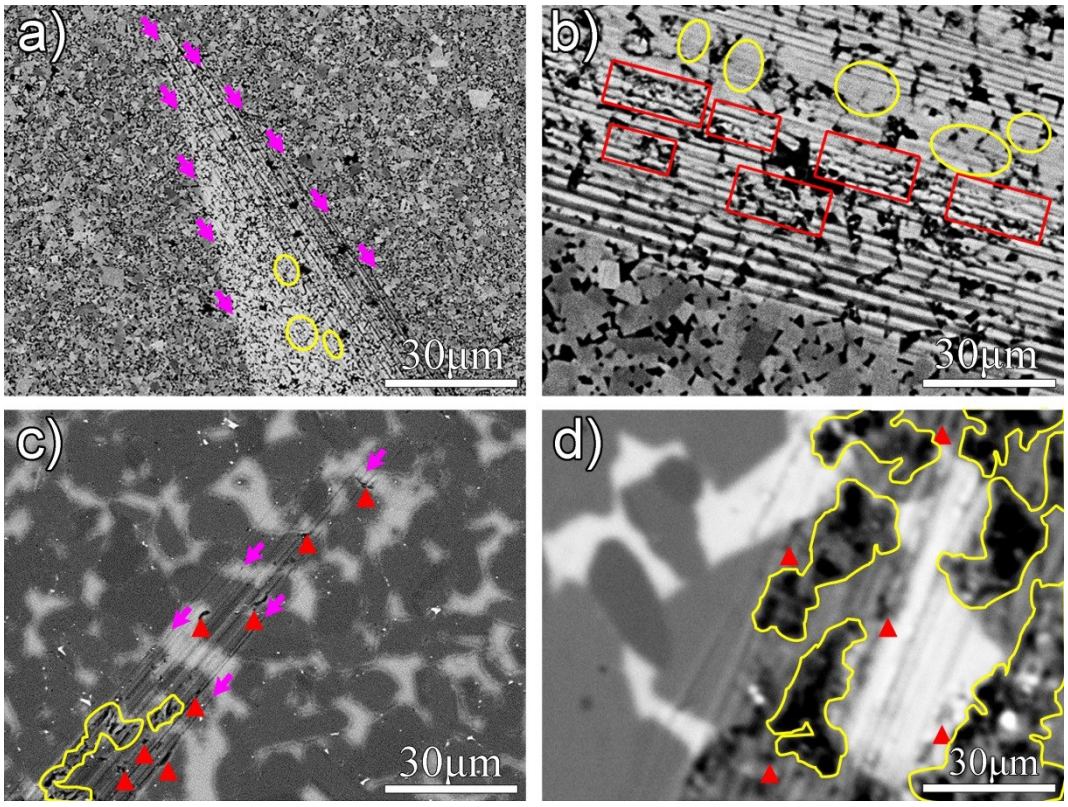

Fig. 6 Surface morphology of the creep feed plunge grinding trace: (a) and (b) for WC/Co; (c) and (d) for RB-SiC/Si

As is illustrated in Fig. 7, three obvious stages of material removal can be found. At the beginning, a limited number of diamond grits participated in the material removal at a smaller depth of cut. Then, more diamond grains were involved in cutting with the increase of grinding depth. As the cutting depth reached about 600 nm for WC/Co, the dislodgement of WC grains appeared before it was crushed at about 1.5 μm. As the depth of cut for a protruded grit become greater than the critical depth which was measured to be lower than 65 nm for RB-SiC/Si, the grinding process entered into the ductile to brittle stage, and obvious pits can be found in the grinding trace due to the brittle fracture of workpiece material. Afterwards, the material removal mode transferred into total fragmentation stage with the further increase of grinding depth.

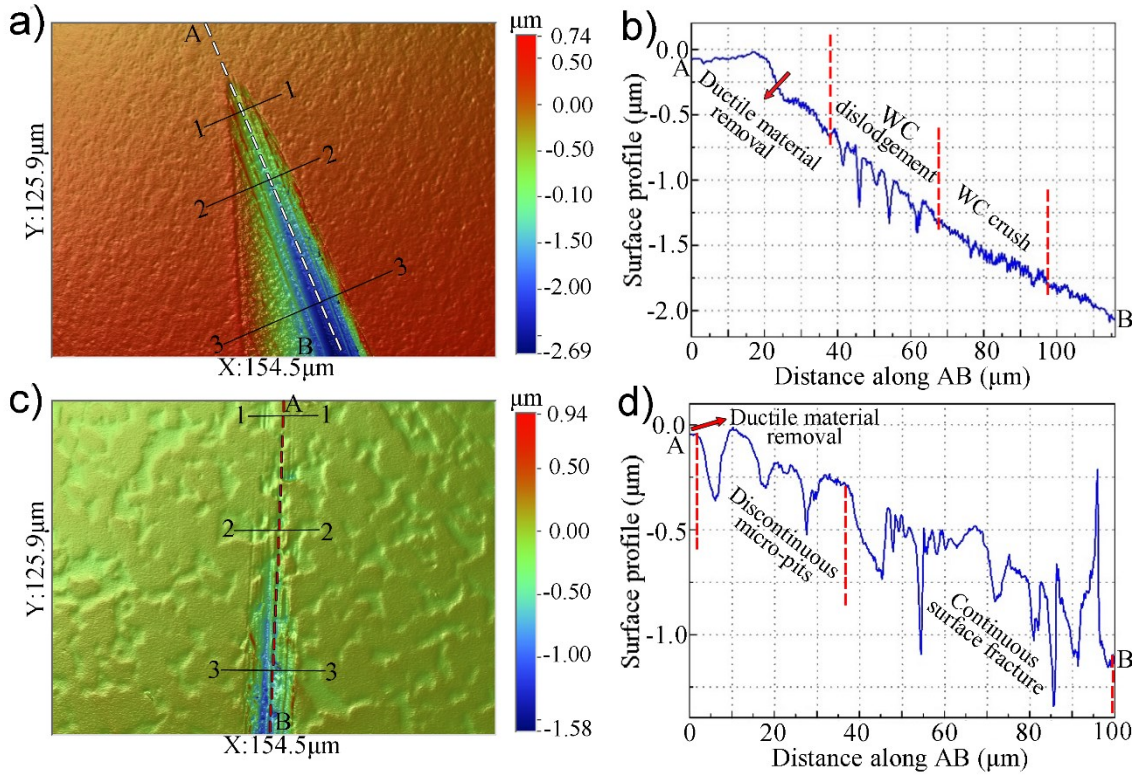

Fig. 7 Surface topography and profile of plunge micro-grinding trace measured by WYKO: (a) and (b) for WC/Co; (c) and (d) for RB-SiC/Si

The cross-sectional profiles of the plunge grinding trace at varied position is shown in Fig. 8. As can be seen from Fig. 8(a), the cross-sectional profile at the very beginning of grinding indicated obvious extrusion between different diamond grits. With the increase of grinding depth, the cross-sectional profile remained similar. The cross-sectional profile for RB-SiC/Si bear much variation, shown in Fig. 8(b). At the initial position, only several diamond grits participated in the material removal, and both Si and SiC experienced ductile removal stage. However, the phase boundaries between SiC and Si were fragile and fracture occurred there, leaving some non-continuous pits. Considering the stochastic distribution of diamond grits and phase boundaries of SiC and Si, non-regular surface fracture occurred at larger cutting depth and the surface morphology also changed randomly.

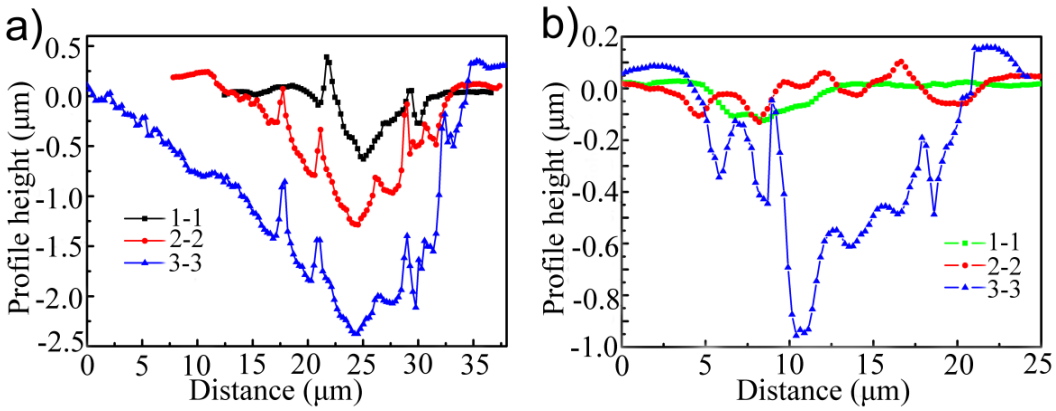

Fig. 8 Cross section profile of plunge micro-grinding trace at varied position indicated in Fig. 7: (a) WC/Co, (b) RB-SiC/Si

Obvious wheel wear occurred during the grinding process and the materials microstructure should also have a great influence on the wear of diamond grinding wheel. As can be seen from Fig. 9(a) and (b), the diamond grits that involved in material removal experienced obvious wear, including grain dislodgement, surface flattening and splintering. It can also be easily seen that the

protruded height of diamond grits is in random and stochastic distribution. Compared with the fresh sharp grains located aside, the surface profile of worn grits was found to be non-regular, shown in Fig. 9(c). The profile indicates that flattening and splintering occurred to diamond grits with a higher protruded height. The wear would lead to the decrease of protruded height of diamond grains. Then, the actual cutting depth for the individual grit would decrease, so the material removal mode was dependent on the depth of cut and the diamond grits wear simultaneously.

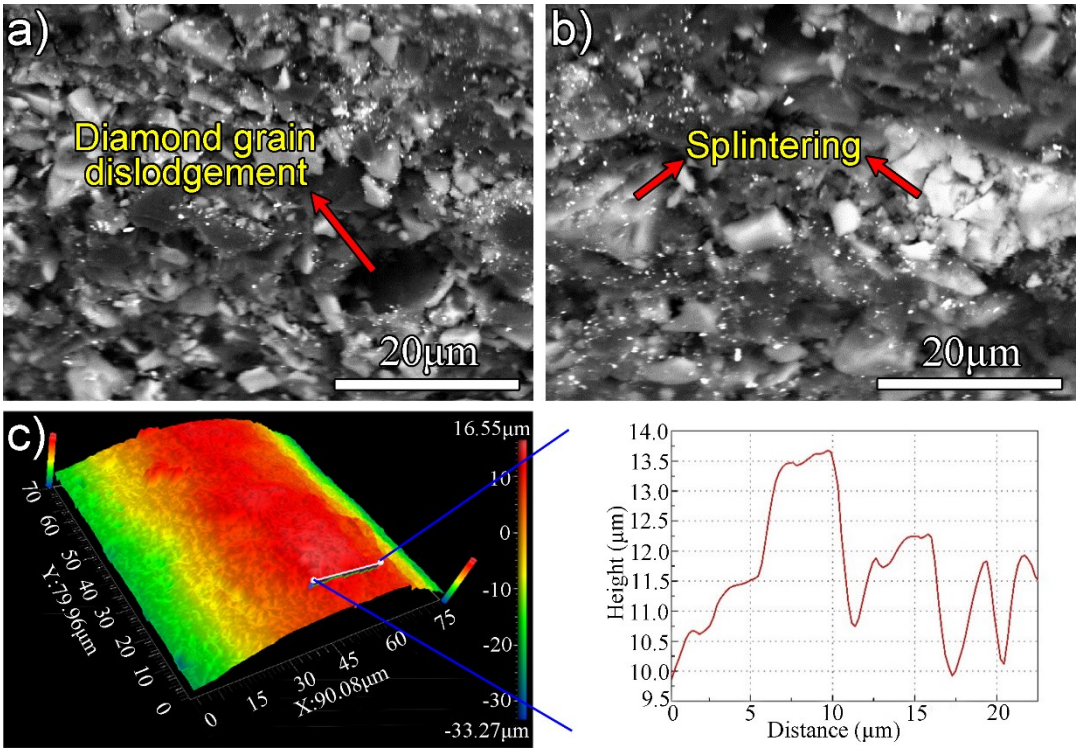

Fig. 9 (a) and (b) SEM surface morphology of the diamond grits of 1500# wheel after grinding; (c) surface profile of the diamond grits after creep-plunge grinding measured by ZYGO

4. Discussion

High pressure induced phase transformation (HPPT) for both Si and Co under indentation has been reported previously [12, 29, 34, 35]. There is no doubt that phase transformation would lead to the change in volume and have a great influence on the bond strength between the hard particles and

binders. Phase transformation of both Si and SiC was identified in the previous study [34, 35, 36], and this would contribute to the fracture of phase boundaries under micro-grinding. Through the indentation results, it could be deduced that the pop-out effect of brittle Si near the phase boundaries was resulted from the phase transformation. Furthermore, the finer microstructure and ductile Co binder of WC/Co contributed to the plastic deformation and improved mechanical properties [16].

In grinding of brittle ceramics, the critical depth of cut d_c for hard and brittle materials was given as following [2, 17, 37, 38]:

$$d_c = 0.15 \cdot \left(\frac{E}{H}\right) \cdot \left(\frac{K_c}{H}\right)^2 \tag{1}$$

Where E is the elastic modulus, H is the hardness, and K_c is the fracture toughness. Compared with the grinding depth a_e, a simplified surface generation condition was achieved:

$$\text{Plastic deformed surface: } a_e < d_c \tag{2}$$

$$\text{Fractured surface: } a_e \geq d_c \tag{3}$$

Based on the mechanical properties given in Table 1, the calculated critical depth of cut for WC/Co and RB-SiC/Si composites was 1.643 μm and 37.6 nm， respectively. This is consistent with the experimental results, shown in Fig. 7.

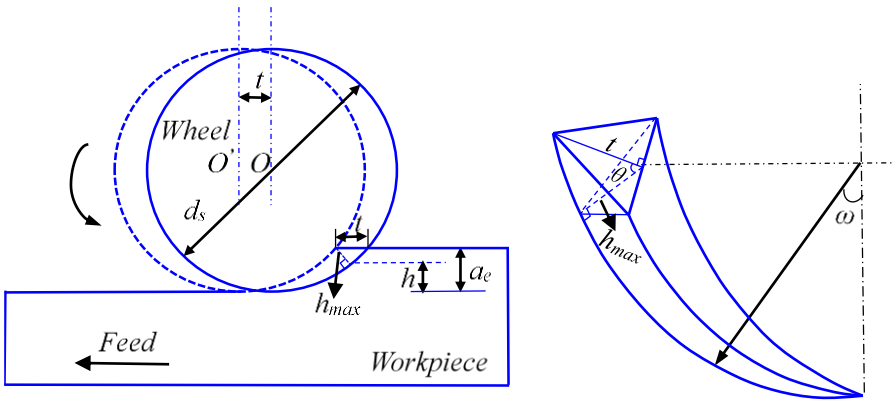

Fig. 10 Illustration of the generation and geometry of the maximum undeformed chip

Nevertheless, it should be noted that the criterion between the surface generation and material removal mode should be distinguished. The generation and geometry of the undeformed cutting chips is illustrated in Fig. 10. The maximum undeformed chip h_{max} is generated related to material properties could be achieved based on the following relation [22]:

$$h_{\max} = \left(\frac{E_1}{E_2}\right)^{0.548}\left[\frac{4}{C \cdot r}\left(\frac{v_w}{v_s}\right)\left(\frac{a_e}{d_s}\right)^{1/2}\right]^{1/2} \tag{4}$$

Where E_1 is the elasticity modulus of the wheel (GPa), E_2 is the elasticity modulus of the workpiece material (GPa), C is grit number per unit area in wheel, r is the chip width-to-thickness ratio, v_w is workpiece speed, v_s is the wheel speed, a_e is grinding depth, d_s is the equivalent wheel diameter. Based on the above analysis, the material removal mechanism in present work was expressed as following:

$$\text{Ductile material removal mode: } h_{\max} < d_c \tag{5}$$

$$\text{Brittle material removal mode: } h_{\max} \geq d_c \tag{6}$$

As is shown in Fig. 10, the maximum undeformed chip thickness occurred at a certain height (h) from the machined surface. What should be noted was that, even though the requirement of equation (6) might be met, the crack length (c) might not reach the machined surface ($c<h$), so it was not enough to affect the surface profile generated.

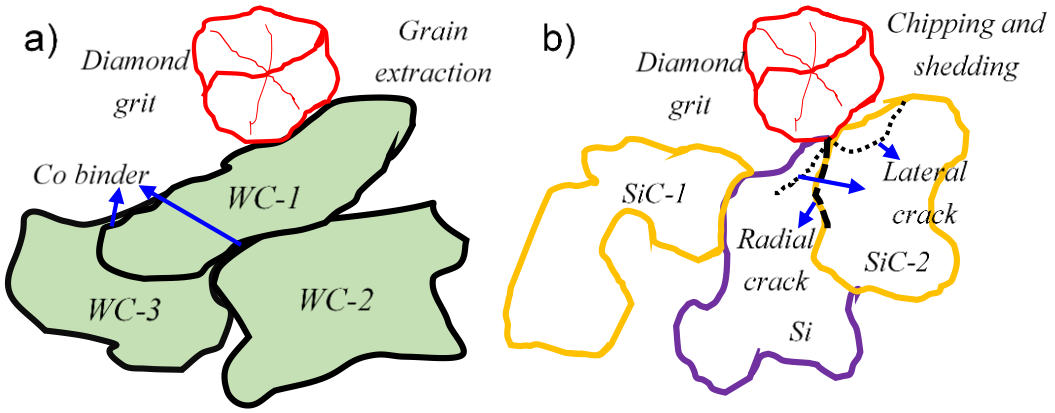

Fig. 11 Grain dislodgement mechanism for (a) WC/Co, (b) RB-SiC/Si

In the present work, plastic deformation occurred firstly under the pressure of diamond grits for both WC/Co and RB-SiC/Si, with diamond grits sliding and scratching on the material surface. This corresponds to the stage of ductile material removal. In ultra-precision machining of monocrystalline and single phase materials, three stages of material removal were often discussed: ductile, ductile to brittle and brittle material removal [2, 24, 39, 40]. Nevertheless, there existed another stage for WC/Co and RB-SiC/Si composites under the dynamic pressure of diamond grit, namely grain dislodgement, if the binder effect was taken into account in machining composites. Combining the results of indentation test and the plunge micro-grinding, it is quite reasonable to say that the material dislodgement mechanism for WC/Co and RB-SiC/Si composites are different. Specifically, hard particle dislodged from the surrounding binders under the dynamic pressure of diamond grit for WC/Co. While for RB-SiC/Si, lateral crack firstly formed and induced, then shedding of these fractured parts from machined surface occurred. Fig. 11 illustrates the two different grain dislodgement mechanism.

During grinding of brittle materials, the radial crack was responsible for surface roughness while the lateral crack contributed to the material removal. According to [41-43], the cutting force f_g,

the tangent cutting force f_{gt}, the normal cutting force f_{gn} of a single grit and grinding specific energy k_t was expressed as follows:

$$f_{gt}(\omega) = k_t \cdot A_c(\omega) \tag{7}$$

$$f_{gn} = \frac{1}{\mu} \cdot f_{gt} \tag{8}$$

$$k_t = \frac{f_{gt} \cdot v_s}{a_e \cdot v_w \cdot b(\omega)} \tag{9}$$

Where $A_c(\omega)$ is the cross-section area of chip, ω is the angle of the grit from the engaging position, $b(\omega)$ is the width of chip relative to ω, and μ is a constant. From equations (7) and (8), it can be seen that both of the tangential and normal grinding force will increase with the increasing depth of cut. As the values become greater than the fracture strength, surface fracture will be induced, described by the following equations [27, 44]:

$$\sigma_t = k_t > \sigma_f = \left(\frac{2 \cdot E \cdot \gamma_g}{(1-\upsilon^2) \cdot \pi \cdot c} \right)^{1/2} \tag{10}$$

$$\sigma_n = \frac{1}{\mu} \cdot k_t > \sigma_f = \left(\frac{2 \cdot E \cdot \gamma_g}{(1-\upsilon^2) \cdot \pi \cdot c} \right)^{1/2} \tag{11}$$

Where σ_t is the tangent stress exerted by diamond grit, σ_n is the normal stress exerted by diamond grit, σ_f is the critical fracture stress of workpiece material, γ_g is the specific surface energy of the hard grain, υ is the Poisson's ratio.

For RB-SiC/Si, as the grinding force reached the fracture strength of the workpiece material, lateral and radial crack would be induced. Discontinuous cracks occurred along the same trace of a diamond grit, which was attributed to the stochastic and random distribution of diamond grits in grinding wheel, as well as the extension of obvious phase boundaries. The existing phase boundaries

between SiC and Si would weaken the surface strength for RB-SiC/Si composites, and it would promote the edge chipping under the dynamic pressure of grits. Besides, the pop-out effect caused by the phase transformation under grinding force should also be considered. Both will prompt the chipping of surface material. For WC/Co, Co binder is much softer compared with hard particle, and then it will be removed more easily and quickly. The non-uniform removal would result in the reduction of binding force between the surface hard phase and the nearby binder. The dislodgement condition of hard grains from binder in composites could be determined based on the following equation [6, 45]:

$$\left(\frac{2\cdot L\cdot \gamma_i}{\gamma_g}\right)+\left(\frac{\tau\cdot L^2}{2\cdot a\cdot \gamma_g}\right)>\phi \tag{12}$$

Where γ_i is the specific fracture energy at the grain boundary, γ_g is the specific surface energy of the grain, τ is assumed to be the constant average shear stress exerted by one grain against the matrix or another grain, $2a$ is the diameter of a grain, L is the length. ϕ is a constant depending on the angle of incidence of the hard particle to the surface. The same mechanism could also help to explain the grit dislodgement wear mode of diamond wheel. Furthermore, the impact and friction effect from the hard particles in the workpiece materials would cause the surface splintering and flattening of diamond grits at the elevated grinding depth. Therefore, the surface profile transferred to be smooth again after the WC crush stage as friction and extrusion effects will rise caused by grit flattening and splintering.

5. Conclusions

In present study, indentation test and high spindle speed grinding (HSSG) of WC/Co and RB-SiC/Si composites were conducted to investigate the surface generation mechanism. The

indentation test indicate that Co binder addition in WC/Co could improve the toughness of bulk materials. However, the phase boundaries became the most fragile point in RB-SiC/Si where evident edge chipping and cracks appeared, considering the influence of phase transformation. The grinding experimental results showed that an increasing depth of cut would deteriorate the surface integrity seriously, and the material removal mechanism differed for WC/Co and RB-SiC/Si composites obviously. It was found that WC/Co composite exhibited three stages of material removal: ductile removal, grain dislodgement and WC particles crush, while ductile removal, phase boundaries crack (along the grinding direction) and chipping occurred for RB-SiC/Si. The mechanics for the different material removal mode were analyzed and discussed based on varied models, which would promote the understanding of ultra-precision machining of advanced ceramic composites. Furthermore, the wheel wear prompted the surface damages, such as surface fracture and binder extrusion.

Acknowledgement

The work was partially supported by the Research Committee of the Hong Kong Polytechnic University (RTRA) and also the National Natural Science Foundation of China (NSFC) (Project No.:51475109).

References

[1] H.Q. Sun, R. Irwan, H. Huang, G.W. Stachowiak, Surface characteristics and removal mechanism of cemented tungsten carbides in nanoscratching, Wear 268 (2010) 1400-1408.

[2] B. Guo, Q. Zhao, M. Jackson, Precision grinding of binderless ultrafine tungsten carbide (WC) microstructured surfaces, Int. J. Adv. Manuf. Technol. 64 (2013) 727-735.

[3] P.G. Neudeck, L.G. Matus, An overview of silicon carbide device technology, AIP Conf. Proc.

246 (1992) 246-253.

[4] Y. Lu, D. He, J. Zhu, X. Yang, First-principles study of pressure-induced phase transition in silicon carbide, Physica B 403 (2008) 3543-3546.

[5] L. Prakash, Fundamentals and general applications of hardmetals. In: V.K. Sarin (Ed.), Comprehensive Hard Materials. Elsevier, Oxford (2014) 29-90.

[6] J. Gao, J. Chen, G. Liu, Y. Yan, X. Liu, Z. Huang, Role of microstructure on surface and subsurface damage of sintered silicon carbide during grinding and polishing, Wear 270 (2010) 88-94.

[7] J.B.J.W. Hegeman, J.T.M. De Hosson, G. de With, Grinding of WC-Co hardmetals, Wear 248 (2001) 187-196.

[8] Y.E. Tohme, Grinding aspheric and freeform micro-optical molds. SPIE (6462) 2007 1-8.

[9] L. Yin, H. Huang, Brittle materials in nano-abrasive fabrication of optical mirror-surfaces, Precis. Eng. 32 (2008) 336-341.

[10] B. Zhang, X.L. Zheng, H. Tokura, M. Yoshikawa, Grinding induced damage in ceramics, J. Mater. Process. Technol. 132 (2003) 353-364.

[11] J. Ni, B. Li, Phase transformation in high-speed cylindrical grinding of SiC and its effects on residual stresses, Mater. Lett. 89 (2012) 150-152.

[12] A. Duszová, P. Hvizdoš, F. Lofaj, Ł. Major, J. Dusza, J. Morgiel, Indentation fatigue of WC–Co cemented carbides, Int. J. Refract. Met. H. 41 (2013) 229-235.

[13] J. Yang, M. Odén, M.P. Johansson-Jõesaar, L. Llanes, Grinding Effects on Surface Integrity and Mechanical Strength of WC-Co Cemented Carbides, Procedia CIRP 13 (2014) 257-263.

[14] S. Agarwal, P.V. Rao, Experimental investigation of surface/subsurface damage formation and material removal mechanisms in SiC grinding, Int. J. Mach. Tools Manuf. 48 (2008) 698-710.

[15] J.C. Aurich, J. Engmann, G.M. Schueler, R. Haberland, Micro grinding tool for manufacture of complex structures in brittle materials, CIRP Ann. - Manuf. Technol. 58 (2009) 311-314.

[16] A.V. Shatov, S.S. Ponomarev, S.A. Firstov, Hardness and deformation of hardmetals at room temperature, In: V.K. Sarin (Ed.), Comprehensive Hard Materials. Elsevier, Oxford (2014) 267-299.

[17] T.G. Bifano, T.A. Dow, R.O. Scattergood, Ductile-Regime Grinding: A New Technology for Machining Brittle Materials, J. Manuf. Sci. Eng. 113 (1991) 184-189.

[18] K. Carlisle, M.A. Stocker, Cost-effective machining of brittle materials (glasses and ceramics) eliminating/minimizing the polishing process. SPIE (3099) 1997 46-58.

[19] Y.H. Ren, B. Zhang, Z.X. Zhou, Specific energy in grinding of tungsten carbides of various grain sizes, CIRP Ann. - Manuf. Technol. 58 (2009) 299-302.

[20] J. Zhang, N. Suzuki, Y. Wang, E. Shamoto, Fundamental investigation of ultra-precision ductile machining of tungsten carbide by applying elliptical vibration cutting with single crystal diamond, J. Mater. Process. Technol. 214 (2014) 2644-2659.

[21] L. Yin, A.C. Spowage, K. Ramesh, H. Huang, J.P. Pickering, E.Y.J. Vancoille, Influence of microstructure on ultraprecision grinding of cemented carbides, Int. J. Mach. Tools Manuf. 44 (2004) 533-543.

[22] S. Agarwal, P. Venkateswara Rao, Grinding characteristics, material removal and damage formation mechanisms in high removal rate grinding of silicon carbide, Int. J. Mach. Tools

Manuf. 50 (2010) 1077-1087.

[23] Z. Dong, H. Cheng, Study on removal mechanism and removal characters for SiC and fused silica by fixed abrasive diamond pellets, Int. J. Mach. Tools Manuf. 85 (2014) 1-13.

[24] L. Yin, E.Y.J. Vancoille, K. Ramesh, H. Huang, Surface characterization of 6H-SiC (0001) substrates in indentation and abrasive machining, Int. J. Mach. Tools Manuf. 44 (2004) 607-615.

[25] X. Wang, X. Zhang, Theoretical study on removal rate and surface roughness in grinding a RB-SiC mirror with a fixed abrasive, Appl. Optics 48 (2009) 904-910.

[26] S. Shimada, N. Ikawa, T. Inamura, N. Takezawa, H. Ohmori, T. Sata, Brittle-ductile transition phenomena in microindentation and micromachining, CIRP Ann. - Manuf. Technol. 44 (1995) 523-526.

[27] R.W. Armstrong, The hardness and strength properties of WC-Co composites, Materials 4 (2011) 1287-1308.

[28] T. Suratwala, L. Wong, P. Miller, M.D. Feit, J. Menapace, R. Steele, P. Davis, D. Walmer, Sub-surface mechanical damage distributions during grinding of fused silica, J. Non-Cryst. Solids 352 (2006) 5601-5617.

[29] M. Bľanda, A. Duszová, T. Csanádi, P. Hvizdoš, F. Lofaj, J. Dusza, Indentation hardness and fatigue of the constituents of WC-Co composites, Int. J. Refract. Met. H. 49 (2015) 178-183.

[30] S. Ndlovu, K. Durst, M. Göken, Investigation of the sliding contact properties of WC-Co hard metals using nanoscratch testing, Wear 263 (2007) 1602-1609.

[31] P.V. Krakhmalev, J. Sukumaran, A. Gåård, Effect of microstructure on edge wear mechanisms

in WC–Co, Int. J. Refract. Met. H. 25 (2007) 171-178.

[32] P. Lee, J. Nam, C. Li, S. Lee, An experimental study on micro-grinding process with nanofluid minimum quantity lubrication (MQL), Int. J. Precis. Eng. Manuf. 13 (2012) 331-338.

[33] H.W. Park, S.Y. Liang, Force modeling of micro-grinding incorporating crystallographic effects, Int. J. Mach. Tools Manuf. 48 (2008) 1658-1667.

[34] H. Huang, J. Yan, New insights into phase transformations in single crystal silicon by controlled cyclic nanoindentation, Scripta Mater. 102 (2015) 35-38.

[35] J. Yan, H. Takahashi, J.I. Tamaki, X. Gai, H. Harada, J. Patten, Nanoindentation tests on diamond-machined silicon wafers, Appl. Phys. Lett. 86 (2005).

[36] Q. Zhang, S. To, Q. Zhao, B. Guo, Amorphization and C segregation based surface generation of Reaction-Bonded SiC/Si composites under micro-grinding, Int. J. Mach. Tools Manuf. 95 (2015) 78-81.

[37] B. Guo, Q. Zhao, Wheel normal grinding of hard and brittle materials, Int. J. Adv. Manuf. Technol. (2015) 1-8.

[38] B. Cho, H. Kim, R. Manivannan, D. Moon, J. Park, On the mechanism of material removal by fixed abrasive lapping of various glass substrates, Wear 302 (2013) 1334-1339.

[39] G. Xiao, S. To, G. Zhang, Molecular dynamics modelling of brittle–ductile cutting mode transition: Case study on silicon carbide, Int. J. Mach. Tools Manuf. 88 (2015) 214-222.

[40] B. Meng, F. Zhang, Z. Li, Deformation and removal characteristics in nanoscratching of 6H-SiC with Berkovich indenter, Mater. Sci. Semiconduct. Process. 31 (2015) 160-165.

[41] H. Chang, J.J.J. Wang, A stochastic grinding force model considering random grit distribution,

Int. J. Mach. Tools Manuf. 48 (2008) 1335-1344.

[42] I.D. Marinescu, H.K. Tönshoff, I. Inasaki, Handbook of Ceramic Grinding and Polishing, Park Ridge, N.J.: Norwich, N.Y, 2000.

[43] S. Malkin, C. Guo, Grinding Technology: Theory and Applications of Machining with Abrasives, Wiley, New York: Industrial Press, 2008.

[44] R.W. Armstrong, W.L. Elban, Hardness properties across multiscales of applied loads and material structures, Mater. Sci. Technol. 28 (2012) 1060-1071.

[45] Z. Xie, R.J. Moon, M. Hoffman, P. Munroe, Y. Cheng, Role of microstructure in the grinding and polishing of α-sialon ceramics, J. Eur. Ceram. Soc. 23 (2003) 2351-2360.